MASCOT simulations
Technical report

Summary

Here we report on the definitions, conventions, methods and tests used and implemented before running the series of MASCOT first bounce simulations. The first section is devoted to the parameters useful for the preparation of the granular bed. Then definitions relative to MASCOT are given in a second section. Finally, plan for the study of the ejecta is presented in the last section.

A) Granular bed

1) Container

The container is a cylinder open on the top, with a diameter equals to 5 times MASCOT's largest dimension (D = 150 cm). This size is thought to be a good compromise between computation time (related to the number of particles) and effect of the sidewall of the cylinder on the simulation's outcomes.

We implemented 3 different heights of cylinder: H = 15, 30 and 40 cm. With H = 15 cm, bottom wall is expected to have an important influence as the area of impact should be depleted from all its particles with the shock wave reaching the bottom of the cylinder. However, this situation is not necessarily unrealistic, if the possibility to land inside a crater is considered. In fact, in a crater, the regolith depth is expected to be smaller and to lie on bare rock [REF]. This situation is compatible with the H = 15 cm case. On the other hand, the outcome is not so obvious with H = 30 or 40 cm. Barnouin et al. (2008) estimated the depth of the fine regolith layer present on Itokawa at 42 ± 1 cm. Moreover, the size of the outer regolith layer is supposed to decrease with the size of the asteroid [REF]. The size estimate for Ryugu being around 980 ± 30 m, which represents XX% of Itokawa's dimensions, a cylinder with a depth of H = 30 or 40 cm appears like a reasonable assumption.

The sidewall and bottom wall are relatively dissipative ($\varepsilon_n = \varepsilon_t = 0.1$), for two reasons. First, the preparation of the granular bed consists in letting randomly distributed grains fall into the cylinder under low gravity. To reduce the time of this already computationally expensive phase, we want to prevent any large bounce of the grains when they hit the bottom of the container, saving the time of the secondary fall it would induce. Secondly, dissipative boundaries may represent what would happen if we were actually simulating a very wide zone of the regolith layer. However, for cases where the boundary may play a non-negligible role in the outcomes (H = 15 cm cases), we also verified the influence of such convention by giving the walls the same ε_n, ε_t as the grains.

Finally, the friction coefficients of the walls are the same as that of the grains.

2) Stiffness of the grains

In our simulations, two key parameters are the normal spring constant k_n and the simulation timestep δt. The value of δt depends on the value of k_n. However, the value of k_n is more difficult to assess, given the poor data available on regolith mechanical properties. A subroutine in pkdgrav provides values for k_n and δt, based on the following equations:

$$k_n \approx m \left(\frac{V_{max}}{x_{max}}\right)^2 \quad \text{and} \quad \delta t = \sqrt{\frac{m}{k_n}}$$

where m is the typical mass of a particle, x_{max} is the maximum overlap allowed when two particles collide (chosen equal to 1% of the smaller radius) and V_{max} is the maximum speed of the particles. After a few tests, the value of V_{max} was assessed at 25 cm/s, which, for a typical radius of 1 cm gives us:

$$k_n \approx 6.6 \times 10^4 \text{ kg/s}^2 \quad \text{and} \quad \delta t \approx 2.9 \times 10^{-5} \text{ s}$$

The typical mass of the grains is assessed by using the typical radius and the density of the grains (the same for all grains). Therefore, as the density of the grains varies depending on the setup (see ...) the value of k_n and δt varies also a little from one setup to the other. However, for a same kind of size distribution (see ...), no significant effects are expected. Conventionally, the tangential spring constant k_t is equal to $\frac{2}{7} k_n$.

The issue is on the value of the normal spring constant k_n. In some cases, it maybe important to match the sound speed of real materials, and k_n can be chosen to control the speed of energy propagation through the grains (Schwartz et al. 2012). However, according to Schwartz et al. (2012): "for many slow-speed granular processes, the computational cost of using a "realistic" value for k_n could be very high, especially for certain materials, and may not result in any worthwhile insight". In fact, in our case, the value of k_n and δt required to match the sound speed are of the order of magnitude:

$$k_n \approx 10^7 \text{ kg/s}^2 \quad \text{and} \quad \delta t \approx 10^{-6} \text{ s}$$

So the issue is, which value of k_n does at best reproduce what we expect of the regolith layer in low gravity... Given the very high number of simulations performed, we stuck to the value of k_n obtained with a maximum speed of 25 cm/s. However, we performed some comparison runs to see how the outcomes of the simulations were affected by the choice of k_n, and found out that, for cases we knew to be affected by boundaries, MASCOT's bounce is enhanced by a greater k_n. However, when small of no bounce occurs, the CoRs are similar in both cases. Other test cases are still running.

3) Coefficients of restitution and friction of the grains

In pkdgrav, the friction particle-particle and particle-wall is characterized with 3 coefficients: static friction coefficient μ_s, rolling friction coefficient μ_r and twisting friction μ_t. Recently, Zhang et al. (in prep.) implemented a new rolling friction model that uses a rolling force spring, which is the

one we are using in this study. It takes as input the 3 friction coefficients above mentioned, plus an additional shape factor β, characterizing the effect of non-spherical grains. We chose to use two different materials with two different angle of repose: gravel and a less frictional material.

$$\text{Gravel (AoR} \approx 39°) \; \mu_s = 1.0 \; ; \; \mu_r = 1.05 \; ; \; \mu_t = 1.3 \; ; \; \beta = 1.0 \; ; \; \varepsilon_n = 0.5 \; ; \; \varepsilon_t = 0.5$$
$$\text{Moderate (AoR} \approx 39°) \; \mu_s = 1.0 \; ; \; \mu_r = 1.05 \; ; \; \mu_t = 1.3 \; ; \; \beta = 0.2 \; ; \; \varepsilon_n = 0.5 \; ; \; \varepsilon_t = 0.5$$

4) Size distribution of the grains

We selected two different types of size distribution. On the one hand we implement a Gaussian distribution of the grains, with a mean value of 1 cm radius, a standard deviation of 30% and a cut-off at 1σ. Fig. 1 shows this cumulative distribution. This distribution is likely too rough compared to that on actual asteroids, however, it has some advantages: it is a poly-disperse distribution (no crystallization), it still contains relatively small grains (minimum 0.7 cm radius), the computational time required to run MASCOT's simulations is acceptable for multi-parameters exploration. It is a good point of comparison with a more realistic power-law distribution and extends our understanding on influence of size distribution on MASCOT's behavior. The radii of this distribution range from approximately 0.7 cm to 1.3 cm. Gundlach and Blum (2013) used available data on thermal inertia of several asteroids to obtain the average regolith grain size range. For Itokawa, they estimated this range to be between 0.7 and 2.4 cm (2.1 +0.3 / -1.4 cm). Therefore, this distribution is still in the range expected for an Itokawa-like asteroid.

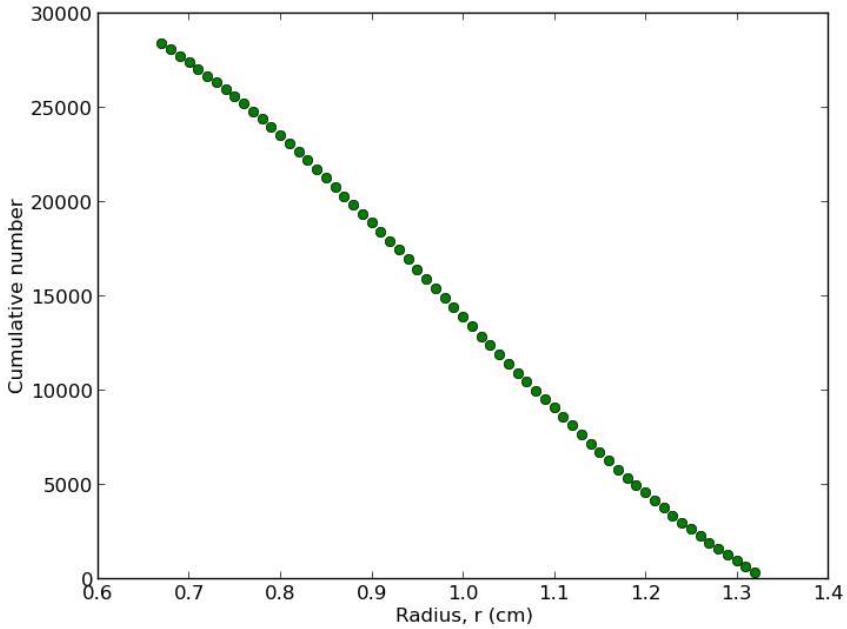

Figure 1 - Cumulative size distribution for Gaussian distribution

On the other hand, we implemented two power-law distributions with different slopes. We took as a reference the asteroid Itokawa, which has been extensively studied in the light of the data and samples collected by the Hayabusa spacecraft. According to Tsuchiyama et al. (2011), the slope of the size distribution varies drastically with the size range of the considered grains. Depending on the sampling mechanism (tapping or spatula), they find a slope of the cumulative

distribution between -2.0 and -2.8, for the size ranges (30µm,100 µm) and (5µm,20µm) respectively. They also propose that -2.8 might be an upper limit, and that the size distribution of mm- and cm-sized grains might have a slope closer to -2.0. We investigated two different slopes of cumulative distribution: -1.7 and -3.0 (the announced values of -2.6 and -4.0 were actually for non cumulative distribution). Referring at Gundlach and Blum (2013), we applied the slope of -1.7 to a size range of 0.2 cm to 2.0 cm. However, in order to limit the computational time in the case of the steeper slope (-3.0), we chose grains ranging from 0.3 to 3.0 cm in radius for this distribution. Figure 2 shows the two power-law distributions.

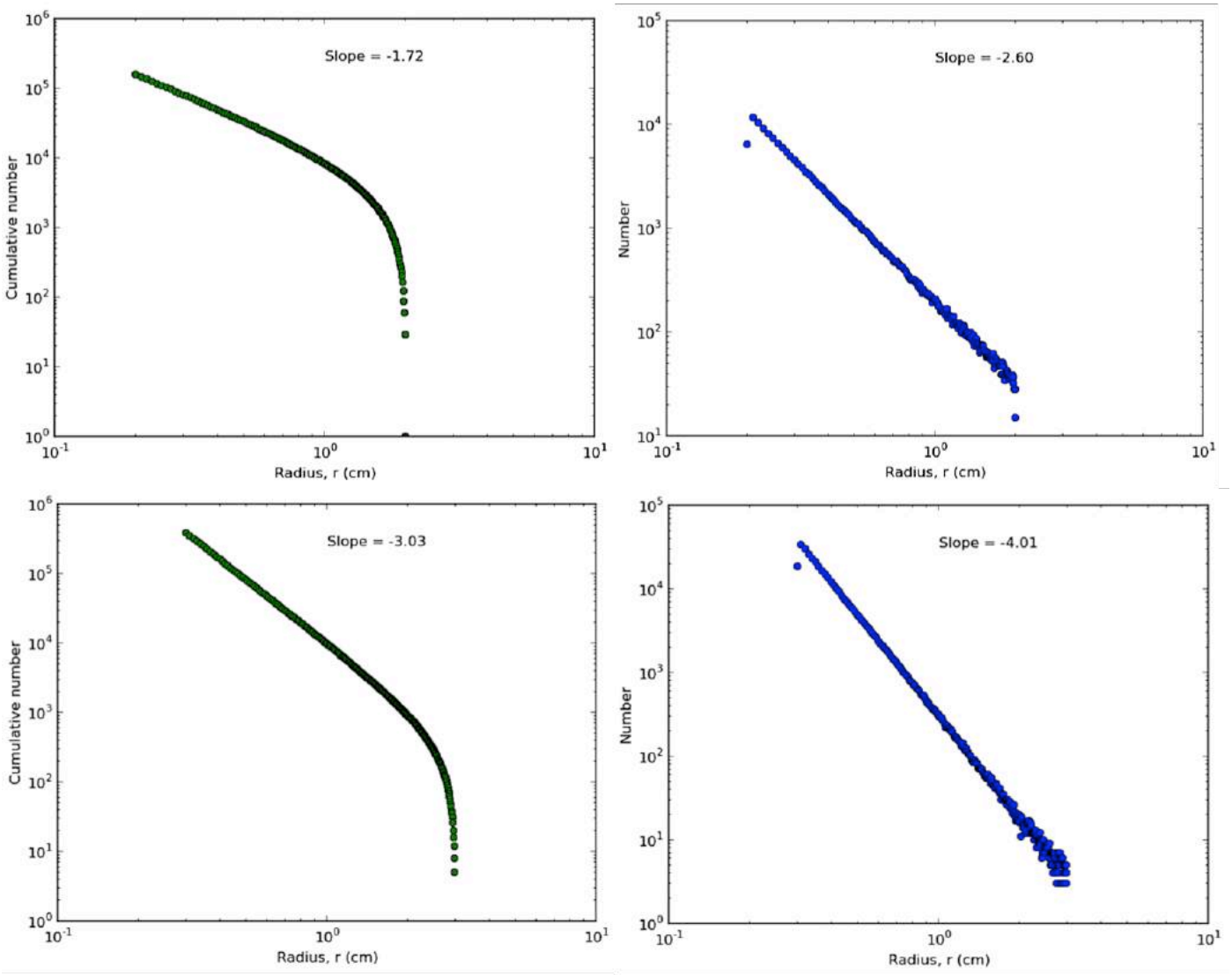

Figure 2 - Cumulative (left) and non-cumulative (right) representations of the power-law distributions

5) Porosity and grains density

The bulk density of Ryugu is assessed at 1280 kg/m^3 [REF], which is consistent with current estimates for C-type asteroids (Carry 2012). Without any additional information available about the regolith layer, we consider the same value for the bulk density of our granular bed. Considering the way the cylinder is filled, the granular system at equilibrium possesses its own micro-porosity (porosity of the order of magnitude of the grains' size, approximately 0.5 cm). We

take into account this porosity to adapt the grains' density, so that our system meets a bulk density of 1280 kg/m^3 inside the cylinder. The porosity level depends on the randomness of the initialization phase. Therefore, the density of the grains will not necessarily be the same for each initial granular bed, even if the size distribution is the same. However, we assume each grain has the same density.

To evaluate the porosity inside the cylinder, we calculate the local porosity inside a sphere that we move through out the cylinder. The dimension and positions of the sphere are so that we do not take into account the particles layer against the walls as well as the very upper layer. Doing so, we prevent from any bias due to the friction against the walls, which creates artificial voids that wouldn't exist if the region were surrounded by grains (which is the undoubtedly case on a real asteroid).

As mentioned previously, the porosity is initialization-dependent. Porosities in our different cylinders range from 2.02 g/cm^3 to 2.51 g/cm^3. Say something about the significance. The densities of the grains derived from these porosities, considering that the bulk density of the bed must be around 1280 kg/m^3, are therefore ranging from 36.7 % to 49 %. The following table summarizes the densities and porosities:

Case			Grains final density ρ_{grain} (g/cc)	Porosity in the cylinder P_{cyl}
R_{grain} = 1 cm SD = 30 %	GRAVEL	H_{cyl} = 15 cm	2.51	49.0 %
		H_{cyl} = 30 cm	2.43	47.4 %
		H_{cyl} = 40 cm	2.40	46.7 %
	MODERATE	H_{cyl} = 15 cm	2.29	44.2 %
		H_{cyl} = 30 cm	2.29	44.2 %
		H_{cyl} = 40 cm	2.31	44.7 %
	GLASS	H_{cyl} = 15 cm	2.14	40.2 %
		H_{cyl} = 30 cm	2.13	39.9 %
		H_{cyl} = 40 cm	2.13	39.9 %
PL -2.5 0.2 -> 2 cm	GRAVEL	H_{cyl} = 15 cm	2.02	36.6 %
		H_{cyl} = 30 cm	2.15	40.5 %
	MODERATE	H_{cyl} = 15 cm	2.02	36.7 %
PL -4.0 0.3 -> 3 cm	GRAVEL	H_{cyl} = 30 cm	2.06	37.7 %

B) MASCOT

1) Basic properties of the lander

- Mass: 10 kg
- Size: 29 x 27.5 x 19.5 cm + MicrOmega
- Touchdown speed: 19 cm/s
- Matrix of inertia with respect to the CoM: $\mathrm{MoI_{CoM}} = \begin{pmatrix} 0.099 & -0.0051 & 0.0019 \\ -0.0051 & 0.0825 & 0.0005 \\ 0.0019 & 0.0005 & 0.121 \end{pmatrix}$ kg m^2
- Moments of inertia: $\mathrm{D} = \begin{pmatrix} 0.081 & 0 & 0 \\ 0 & 0.100 & 0 \\ 0 & 0 & 0.121 \end{pmatrix}$ kg m^2
- Principal axes of inertia: $\mathrm{P} = \begin{pmatrix} -0.27533 & 0.95758 & 0.085034 \\ -0.96102 & -0.27647 & 0.0016687 \\ 0.025107 & -0.08126 & 0.99638 \end{pmatrix}$
- Coefficients of restitution: $\varepsilon_n = 0.6$; $\varepsilon_t = 0.6$
- Coefficients of friction: the same as the grains (maybe not optimal...)

2) Parameters space investigated

- Touchdown speed: 19 cm/s (some cases at 9.5, 4.25 and 2.0 cm/s running)
- Angle of approach: 0° - 15° - 30° - 45° - 60°
- Attitude of approach: flat, on an edge parallel to the velocity direction, on an edge perpendicular to the velocity direction, on a corner
- Spin: no spin - 0.1 rd/s around each principal axis

In total, we have 2 (friction) x 1 (speed) x 5 (angle) x 3 (depth) x 4 (attitude) x 4 (spin) = 480 simulations done. Remain to be done the simulations with different speeds, and with power-law distributions.

3) Interesting output parameters

Here are listed the outputted parameters:

- Collision duration (maybe to be improved, see below)
- Maximum height of the box
- Velocity vector
- Normal, tangential and total speeds
- Rotation vector
- Total rotation rate
- Outgoing angle
- Maximum acceleration
- Normal, tangential, total and structural CoRs

4) Conservation of angular momentum

Before starting the simulations, the conservation of angular momentum of the system was verified with a series of tests. In particular, the version of MASCOT used for the 2015 simulations turned out to be physically wrong. This section describes the changes and tests.

a) Changes made to the code

Ron.

b) Tests

- Dzhanibekov effect

The intermediate axis theorem, also called Dzhanibekov effect, describes the fact that an object with three different principal axes of inertia is unstable if rotated mainly along its second principal axis, while stable when rotated along the first and third axes. The timescale at which the instability becomes visible depends on the ratio of the rotation rate along the intermediate principal axis and the one along the two other principal axes. The explanation of this effect can be directly derived from Euler equations (for details see Ashbaugh et al. (1991)). We create an assembly made of a cylinder glued to a parallelepiped as represented on Fig. 3:

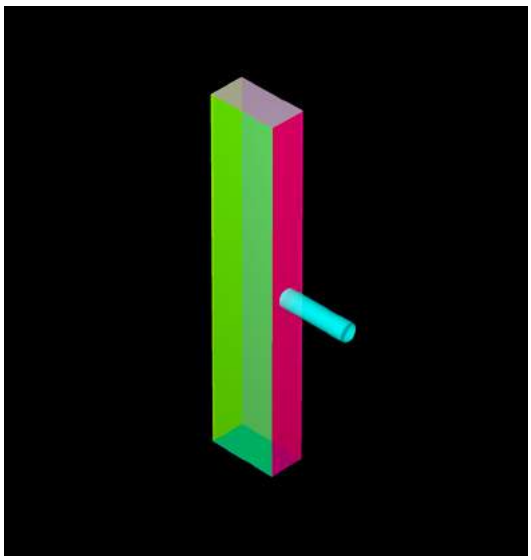

Figure 3 - Walls assembly for the Dzhanibekov test

The cylinder weighs 1g while the parallelepiped is 6 times heavier. The matrix of inertia associated to this assembly is the following:

$$MoI_{cyl} = \begin{pmatrix} \frac{1}{4}m_{cyl}{R_{cyl}}^2 + \frac{1}{12}m_{cyl}h^2 & 0 & 0 \\ 0 & \frac{1}{4}m_{cyl}{R_{cyl}}^2 + \frac{1}{12}m_{cyl}h^2 & 0 \\ 0 & 0 & \frac{1}{4}m_{cyl}{R_{cyl}}^2 + \frac{1}{12}m_{cyl}h^2 \end{pmatrix}$$

$$MoI_{box} = \begin{pmatrix} m_{box}\left(\frac{{c_y}^2 + {c_z}^2}{3}\right) & 0 & 0 \\ 0 & m_{box}\left(\frac{{c_x}^2 + {c_z}^2}{3}\right) & 0 \\ 0 & 0 & m_{box}\left(\frac{{c_x}^2 + {c_y}^2}{3}\right) \end{pmatrix}$$

$$MoI_{tot} = MoI_{cyl} + MoI_{box} = \begin{pmatrix} 209.333 & 0 & 0 \\ 0 & 203.333 & 0 \\ 0 & 0 & 11.333 \end{pmatrix} \text{g cm}^2$$

This particular case satisfies the conditions that are necessary for the Dzhanibekov effect to occur: three different moments of inertia, and a rotation along the cylinder axis, which is the intermediate principal axis of inertia. We make the assembly rotate along its y-axis at $\omega_y = 0.2$ rd/s, with a small perturbation along the x- and z- axes of $\omega_x = \omega_z = 0.02$ rd/s.
As a result, we observe the assembly flipping back and forth along the y-axis, effect visible on Fig. 4 with the change in sign of the y-component of the intermediate principal axis (lying along the axis of the cylinder). Additionally, we verify that the angular momentum is conserved with a precision better than 10^{-5} %.

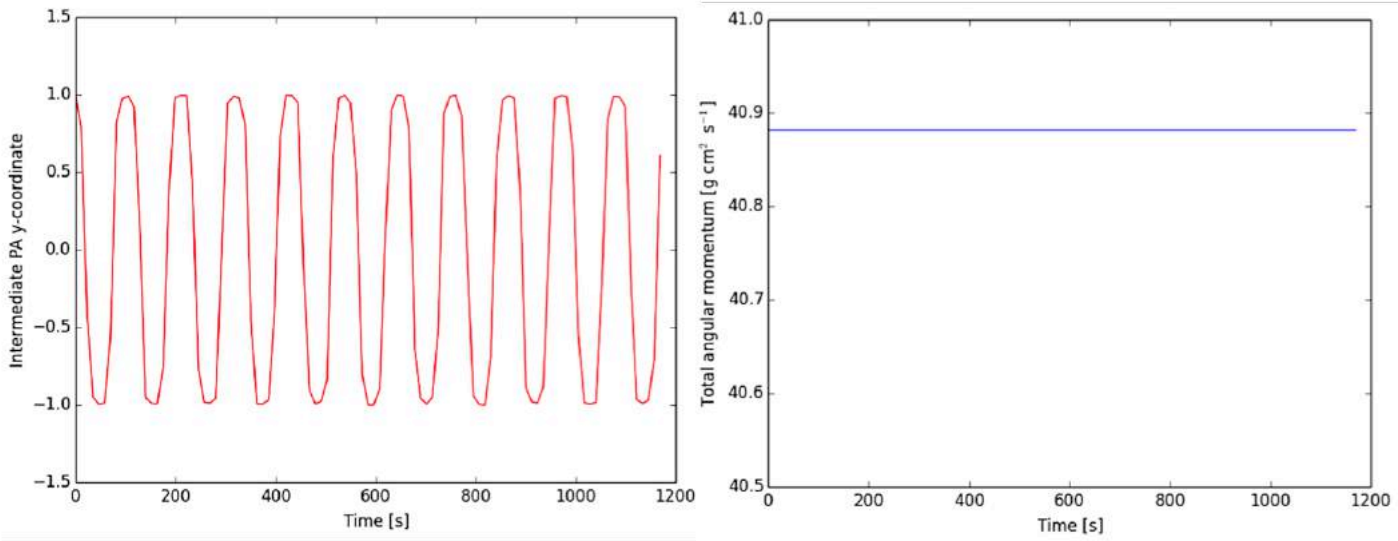

Figure 4 - Left: evolution of the y-coordinate of the intermediate principal axis. Right: Evolution of the angular momentum.

- Spherical wall hitting a particle and vice versa

To check whether the forces applied by a moving wall to a particle, and by a particle to a moving wall was correctly implemented, we performed two simple tests involving a spherical wall and a particle. First, the particle is still. The spherical wall is given a velocity and a spin and hits the particle. Secondly, the wall is still and the spinning particle hits the wall. Figure 5 shows the evolution of the different angular momentums in the two cases.

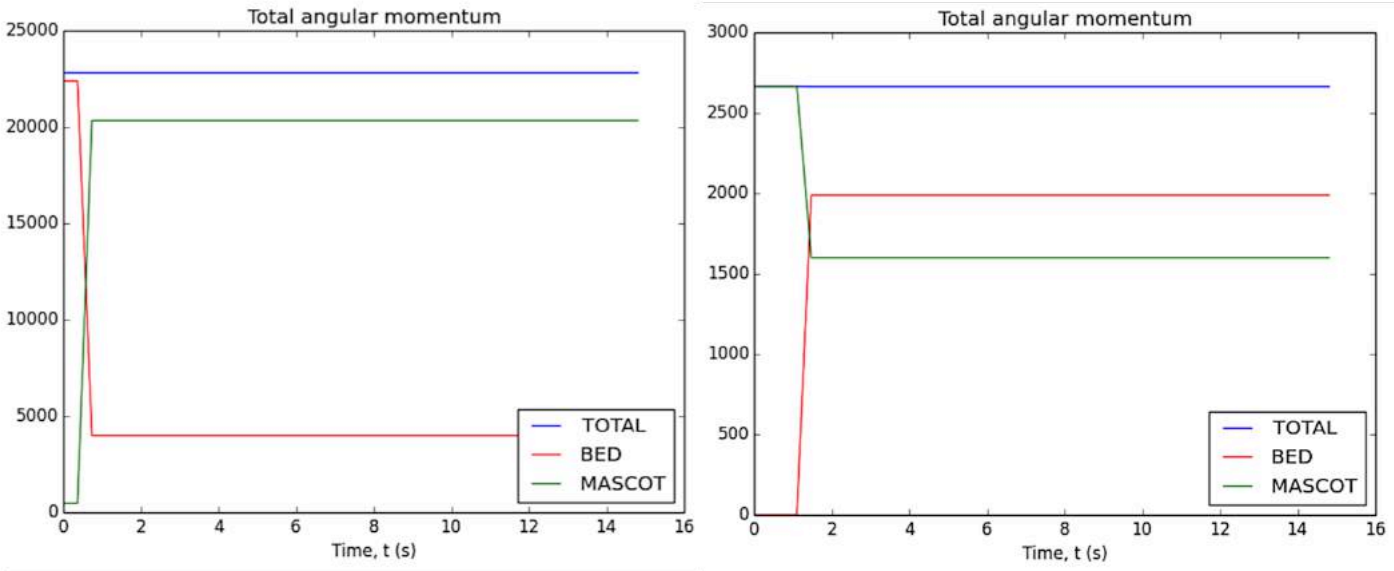

Figure 5 - Left: spinning ball hitting a still spherical wall (g cm² s⁻¹). Right: spinning spherical wall hitting a still particle (g cm² s⁻¹).

- MASCOT hitting a still particle

Before testing on a real case, we perform a last test scenario to verify that the angular momentum is conserved when the real MASCOT hits a particle. We place MASCOT above a still particle in a zero gravity environment, and make it rotate along its first principal axis with an angular velocity of 2.0 rd/s. Once MASCOT hits the particle, we verify that the angular momentum is conserved. Fig. 6 shows the evolution of the angular momentum of the system with time:

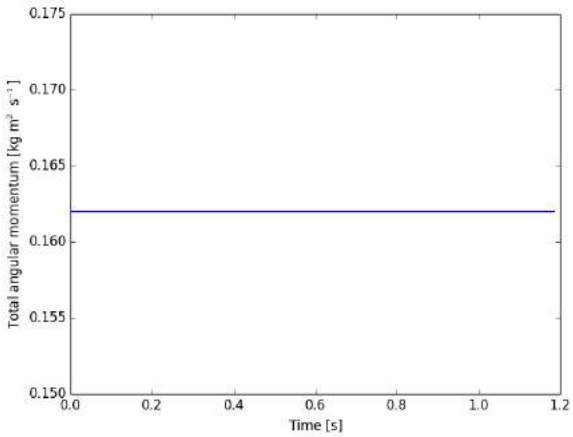

Figure 6 - Total angular momentum of MASCOT + particle as a function of time

- Real case test

Finally, we test the conservation of angular momentum on a real case simulation, where MASCOT impacts a granular bed with a vertical velocity of 50 cm/s and a spin along its third principal axis of 5 rd/s. The granular bed is composed of 28375 particles with a mean radius of 1.0 cm, a standard deviation of 30%, and a cut-off at 1σ. This bed has gravel-like friction parameters and is 15 cm high. For the purpose of this test, we adapted the code so that it was possible to give a finite mass to the cylinder (normally of infinite mass). The mass given to the cylinder was two orders of magnitude higher than the total mass of the particles. As shown on Fig. 7, we found a

little dependence in time of the total angular momentum. This might be due to the precision of the integrator used to calculate the motion of the box (Euler method -- see if Ron advanced on that). However, for the purpose of short simulations, we estimate this variation of angular momentum as negligible (see evolution of total angular momentum on left panel).

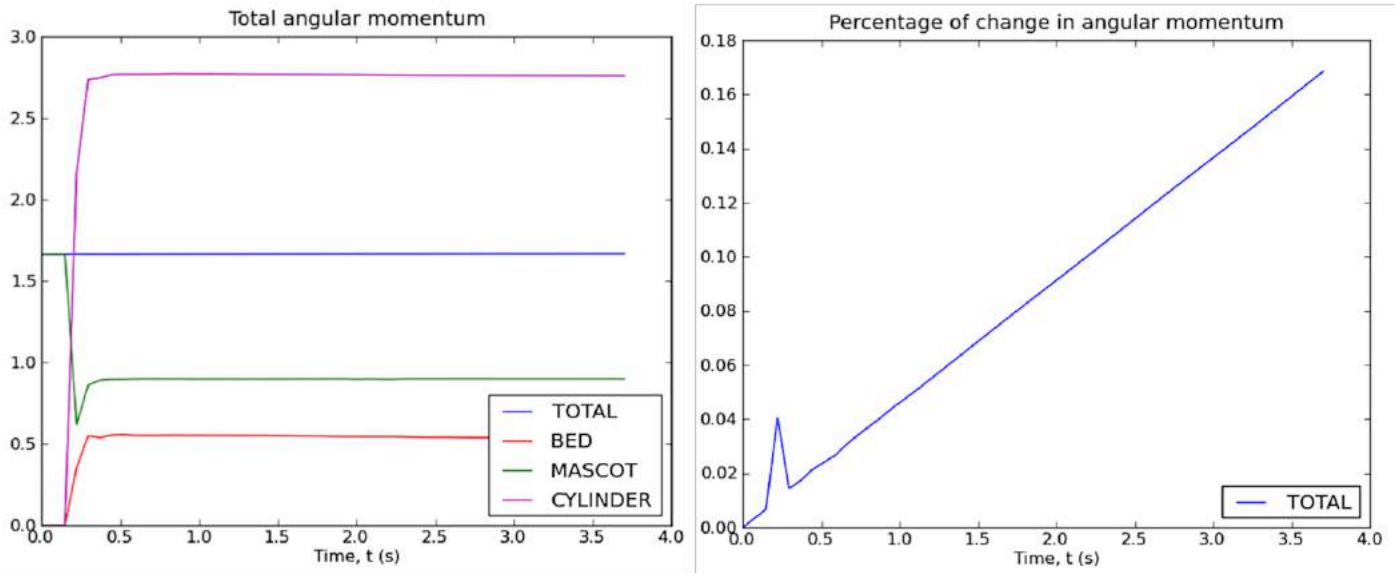

Figure 7 - Left: angular momentum (kg m² s⁻¹) of the different part of the system, and total. Right: percentage of change in total angular momentum (compared to t=0) as function of time

5) Incoming and outgoing angle

a) Definition of the time of first and last contacts

The first contact between MASCOT and the surface can be easily identified. In fact, an important discontinuity in the velocity profile of MASCOT's CoM reflects the transition between uniform speed and contact. The time of first contact is the step just before the discontinuity occurs.

As we do not consider MASCOT as a point mass, the contact between the lander and the surface will very likely last a few time steps (in contrast with the impact of a single point-mass that would be instantaneous). Thus the time of last contact will not necessarily be the same as the one of first contact. It is not so easy to determine whether and when the lander lifts from the surface and starts bouncing. For this, we used different criteria:

- MASCOT does not bounce when: 1) its normal speed remains above 0.01 cm/s during the whole simulation; 2) the slope of its CoG altitude as function of time is always negative 3) the same slope is too shallow.
- MASCOT bounces when: 1) it reaches the height chosen to determine the input parameters (3 cm above the height of the CoG at first contact); 2) it does not reach this point but its trajectory has a slope steep enough to say it is actually bouncing (the lander might still be embedded in the granular bed but still lifting up).

/!\ This method is maybe not optimal... But for the moment I cannot see a general criteria that would help determining whether MASCOT has just lifted or not.

b) Angles calculation

It is very likely that MASCOT will arrive at the surface of the targeted asteroid with a certain angle with respect to the normal to the surface. The trajectory of MASCOT is represented by the one of its CoM. However, as we do not consider MASCOT as a single point-mass, the incoming angle will calculated as the angle between *a)* the vector joining the position of the CoG at a certain height (3 cm above the CoG at first contact on Fig. 8 left panel) and its position when MASCOT first touches the surface of the asteroid, *b)* the normal to the surface.

Once again, as MASCOT is not considered as a single point-mass, the position of the CoG when the lander lifts up and loose contact with the surface will not necessarily correspond to its position at first contact (defined in Fig. 8 left panel). We choose to define the outgoing angle as the angle between *a)* the vector joining the position of the CoG when MASCOT satisfies one of the criteria above mentioned, *b)* the normal to the surface. If MASCOT is considered as not bouncing, its outgoing angle is 90°.

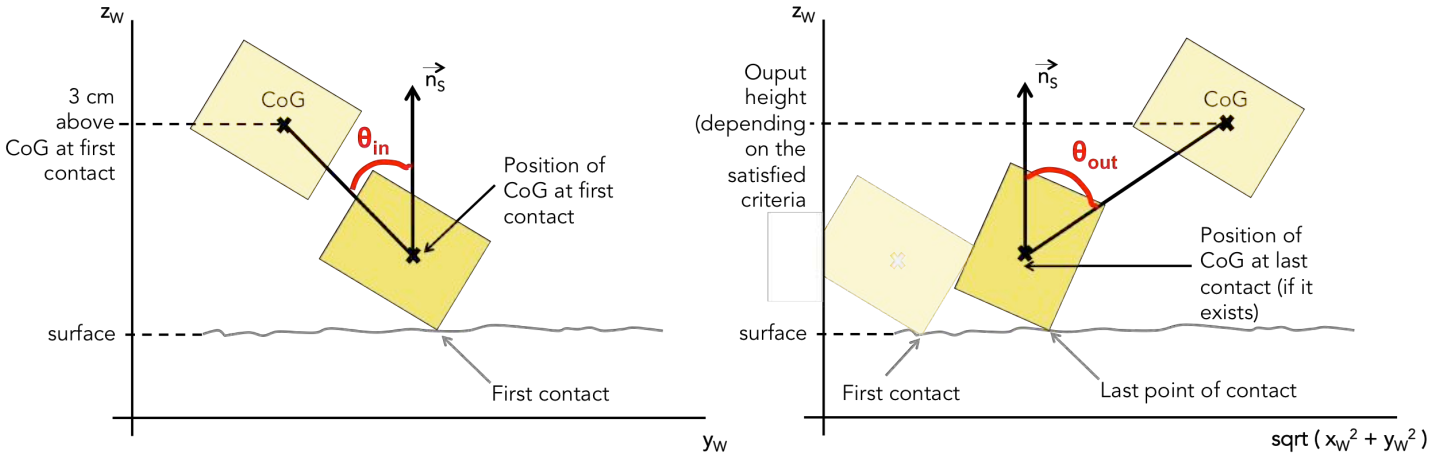

Figure 8 - Incoming and outgoing angles definition

Note that the simulations are initiated so that the lander arrives at the surface in the (y_W , z_W) plane. However, there is no particular reason for MASCOT to remain in that plane while bouncing. The outgoing angle is therefore defined in the $(\sqrt{x_W^2 + y_W^2}, z_w)$ plane.

6) Coefficients of restitution

Several types of coefficient of restitution (CoR) can be obtained from the simulations. These coefficients will be calculated using data from the initial and final states of the bounce, obtained at distinct times that do not necessarily correspond to the beginning and the end of the simulation. For this, a threshold will be defined, for example, the initial state will be when the CoG is at 10 cm above the surface before touching, and the final state will be at 10 cm above the surface after bouncing (see Fig. 1 and 2).

Normal, tangential and total coefficients of restitution are defined as follows:

$$CoR_N = -\frac{V_{out} \cdot n_S}{V_{in} \cdot n_S}$$

$$CoR_{TG} = \frac{\| V_{out} \times n_S \|}{\| V_{in} \times n_S \|}$$

$$CoR_{TOT} = \frac{\| V_{out} \|}{\| V_{in} \|}$$

V_{in} and V_{out} are respectively MASCOT's velocities at above-defined initial and final states of the bounce, with respect to the world frame.

The definition of the structural CoR follows the one described in [Biele et al. REF]. This coefficient...

Structural CoR is defined as follows:

$$CoR_{STR} = \sqrt{\frac{K_{out}}{K_{in}}}$$

$$K_{in/out} = \frac{1}{2} M (v_x^2{}_{in/out} + v_y^2{}_{in/out} + v_z^2{}_{in/out}) + \frac{1}{2} \bar{\omega}_{in/out}^T \cdot \bar{\bar{J}}_{CoM} \cdot \bar{\omega}_{in/out}$$

$\bar{\bar{J}}_{CoM}$ is MASCOT's inertia tensor with respect to the CoM, $\bar{\omega}_{in/out}$ is the direction of the normed rotation vector.

7) Coordinate systems (used for Euler angles - so not used yet)

We define 3 coordinate systems:

- World frame: O_W = (0,0,0) and X_W = (1,0,0) ; Y_W = (0,1,0) ; Z_W = (0,0,1)

Let us note C_X, C_Y, C_Z the coordinates of MASCOT's CoM, and V_X, V_Y, V_Z the normalized direction of MASCOT's edges respectively along its X, Y and Z direction, all expressed in the world frame:

- Mascot fixed frame: O_M = (C_X,C_Y,C_Z) and X_M = V_X ; Y_M = V_Y ; Z_M = V_Z

We note P_X, P_Y, P_Z the direction of the MASCOT's principal axes of inertia expressed in the world frame:

- Principal axes of inertia frame: O_M = (C_X,C_Y,C_Z) and X_{PoI} = P_X ; Y_{PoI} = P_Y ; Z_{PoI} = P_Z

8) Euler angles [NOT SOLVED YET]

This section explains the convention chosen to express MASCOT's 3 Euler angles. By knowing the attitude of the lander after the bounce, we will be able to restart simulations after the bounce in order to measure how long it takes to the lander to bounce a second time, how far it can go, etc.

The fixed coordinate system (world) is noted (x_W, y_W, z_W). In pkdgrav we define a rectangular wall by an origin and 2 perpendicular vertices giving the orientation and size of the rectangle. Once the simulation is over, we can access the location of the origin and direction of each vertex at every time step. We are going to use the origin and the 2 vertices attached to MASCOT's bottom wall (plus the cross product to make an orthonormal coordinate system) as the body-fixed system. This system expressed in the world system is noted (x_M, y_M, z_M).

We refer to:
http://geom3d.com/data/documents/Calculation=20of=20Euler=20angles.pdf

To obtain the Euler angle (α, β and γ) we have to perform 3 rotations:

1) Rotate around z_M by an angle α
2) Rotate around the transformed x_M axis (usually noted x') by an angle β
3) Rotate around the transformed z_M axis by an angle γ

To calculate α, the new position of x_M is $x' = z_M \times z_W$ and:

$$\tan(\alpha) = \frac{x' \,.\, y_M}{x' \,.\, x_M}$$

To calculate β:

$$\tan(\beta) = \sqrt{\frac{(z_M \,.\, x_W)^2 + (z_M \,.\, y_W)^2}{z_M \,.\, z_W}}$$

To calculate γ:

* IF $\sqrt{(z_M \,.\, x_W)^2 + (z_M \,.\, y_W)^2} \neq 0$, then:

$$\tan(\gamma) = z_M \,.\, x_W$$

* IF however, $\sqrt{(z_M \,.\, x_W)^2 + (z_M \,.\, y_W)^2} = 0$, then:

$$\alpha = 0$$
$$\beta = 0$$
$$\tan(\gamma) = -\frac{x_M \,.\, y_W}{x_M \,.\, x_W}$$

9) Acceleration profile

Murdoch et al. (in prep.?) showed with experiments in droptower that the actual acceleration peak, in their conditions, due to a shock in low gravity environment would last approximately 0.2 s. Based on that, we defined our period of output at approximately 0.07s (2500 time steps, step duration = 2.96e-5 s), so that we were sure to see the actual peak of acceleration due to the contact with the surface.

C) Ejecta

1) Parameters

We use the same characterization of the ejecta than that proposed by Housen and Holsapple (2011) for high velocity impacts. An ejected particle is defined by a launch position and an ejection velocity. The launch position is the distance between the location of the particle when it passes the mean surface height and the location of the impact. In our case, we are facing a low velocity impact. Therefore, the impact cannot be considered as instantaneous and the definition of the impact point is not so straightforward. We defined previously the times of first and last contact of the lander with the surface. As a reference, we assume the impact occurs at the mean location of the CoM between its location at time of first and last contact. In addition, the ejection velocity is defined as the velocity of the particle when it reaches its launch position. Fig. 9 illustrates the two parameters:

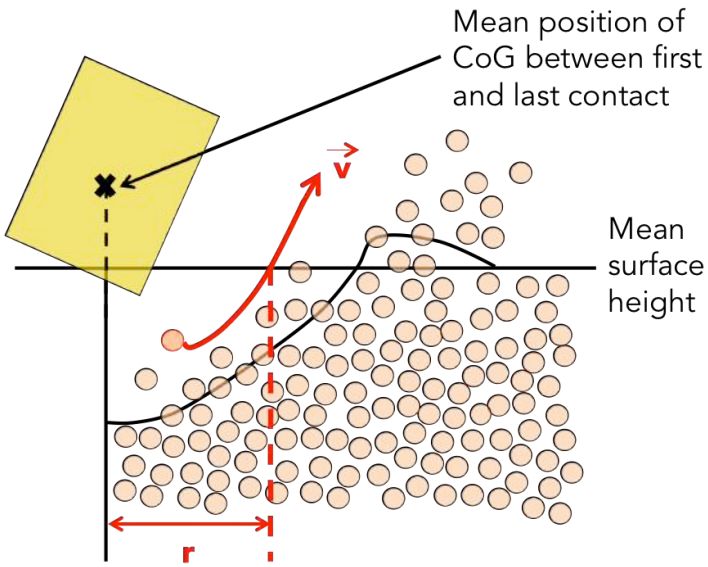

Figure 9 - Ejecta parameters. We note r the launch position and v the ejection velocity.

2) Quantification and adimensionalization

In order to quantify the amount of ejecta, we stick to the two ways presented in Housen and Holsapple (2011):

- Ejection velocity function of launch position
- Total mass ejected with velocity greater than ejection velocity, function of ejection velocity

We also add the identification of the depth of the "crater" formed (by looking at the initial position of the particles considered as ejecta) and its approximate area (needs to be imporved).